International Journal of Biological Macromolecules 151 (2020) 609–617

Contents lists available at ScienceDirect

International Journal of Biological Macromolecules

journal homepage: http://www.elsevier.com/locate/ijbiomac

Tyr320 is a molecular determinant of the catalytic activity of β-glucosidase from *Neosartorya fischeri*

Ramasamy Shanmugam [a,1], In-Won Kim [a,1], Manish K. Tiwari [a,1], Hui Gao [a], Primata Mardina [a], Devashish Das [a], Anurag Kumar [a], Marimuthu Jeya [a], Sang-Yong Kim [b], Young Sin Kim [a], Jung-Kul Lee [a,*]

[a] Department of Chemical Engineering, Konkuk University, Seoul 05029, Republic of Korea
[b] Department of Food Science and Biotechnology, Shin-Ansan University, Ansan 15435, Republic of Korea

ARTICLE INFO

Article history:
Received 22 June 2019
Received in revised form 9 February 2020
Accepted 11 February 2020
Available online 12 February 2020

Keywords:
Catalytic efficiency
β-Glucosidase
Substrate affinity
π-Sigma interaction
MD simulation

ABSTRACT

β-Glucosidases (BGL) are key members of the cellulase enzyme complex that determine efficiency of lignocellulosic biomass degradation, which have shown great functional importance to many biotechnological systems. A previous reported BGL from *Neosartorya fischeri* (NfBGL) showed much higher activity than other BGLs. Screening the important residues based on sequence alignment, analyzing a homology model, and subsequent alteration of individually screened residues by site-directed mutagenesis were carried out to investigate the molecular determinants of the enzyme's high catalytic efficiency. Tyr320, located in the wild-type NfBGL substrate-binding pocket was identified as crucial to the catalytic function of NfBGL. The replacement of Tyr320 with aromatic amino acids did not significantly alter the catalytic efficiency towards *p*-nitrophenyl β-D-glucopyranoside (*p*NPG). However, mutants with charged and hydrophilic amino acids showed almost no activity towards *p*NPG. Computational studies suggested that an aromatic acid is required at position 320 in NfBGL to stabilize the enzyme-substrate complex formation. This knowledge on the mechanism of action of the molecular determinants can also help rational protein engineering of BGLs.

1. Introduction

β-Glucosidases (BGLs) are a type of enzymes present in cellulase mixtures that break down cellulose. BGLs can be detected in bacteria, archaea, and eukarya, with a range of functions [1]. In some bacteria and fungi, they can degrade cellulose to glucose. Cellobiohydrolases and endoglucanases hydrolyze cellulose to produce cellobiose and short-cell oligosaccharides, which can be further hydrolyzed by BGLs to glucose [2,3]. Compared to chemical processes for producing fuels and other chemicals, the biomass conversion can offer higher selectivity, higher yields, and milder operating conditions. However, the commercial application of this promising technology is still limited, mainly due to the high enzyme cost and their low catalytic activity. Highly efficient BGLs could help optimize the commercial use of cellulosic biomass [4]; thus the enzymology of BGLs has been drawing a lot of attention. Various forms of BGLs have been characterized from a variety of organisms, with some showing potential industrial uses [5] including biomass conversion [6] and ethanol production [7]. Several highly thermotolerant enzymes have been characterized from *Thermoascus aurantiacus* [8], *Talaromyces emersonii*, *Paenibacillus polymyxa* [9], and *Penicillium brasilianum* [10]. The reported BGLs tend to have broad specificity, although some with high substrate specificity for *p*NPG have also been reported [11,12].

One strategy for improving the properties of BGLs is to increase their activity through protein engineering. The functionalities of BGLs have been improved by random mutagenesis and site-directed mutagenesis. Glucose production has been enhanced through site-directed mutation of BGLA1, with 1.5- and 1.6-fold higher glucose conversions [12]. BglC from *Thermobifida fusca* with triple mutant (N317Y/L444F/A433V) after random mutagenesis has shown higher stability, with 5 °C higher denaturation temperature [13]. These previous mutational studies aimed to improve enzyme properties for various application. Structural studies, including those on the three-dimensional (3D) structure of *Phanerochaete chrysosporium* BGLA (PcBGLA, 2E3Z), [14] have been performed to establish the reaction mechanisms [15], substrate-binding sites, and activity site recognition of BGLAs [16]. A study by Masayuki et al. [17] revealed the crucial role of Glu191 and Glu407 in the hydrolysis process, using a site-directed mutagenesis approach. However, the mechanism, which governs the molecular determinants that contribute to the catalytic efficiency of BGLs remains to be elucidated.

* Corresponding author at: Department of Chemical Engineering, Konkuk University, 1 Hwayang-dong, Gwangjin-gu, Seoul 05029, Republic of Korea.
E-mail address: jkrhee@konkuk.ac.kr (J.-K. Lee).
[1] These authors equally contributed to this work.

https://doi.org/10.1016/j.ijbiomac.2020.02.117
0141-8130/

In this study, a highly active BGL from *N. fischeri* (NfBGL) NRRL181 was chosen to study the molecular mechanism of its high catalytic efficiency. A crucial residue responsible for its high catalytic efficiency was identified through a systematic screening and verification process including molecular dynamics (MD) simulations and subsequent mutagenesis. Additionally, we confirmed that Tyr320 plays a very important role in the high catalytic efficiency of BGLs by a Molecular Mechanics Poisson-Boltzmann Surface Area (MM/PBSA) approach. The analysis of the NfBGL model docked with *p*NPG showed that Tyr320 interacts with the substrate.

2. Materials and methods

2.1. Materials

The reagents used for PCR were bought from Promega (Madison, WI). The restriction enzymes used in cloning were purchased from New England Biolabs (MA). The expression vector pET28a was obtained from Novagen (Madison, WI). The primers were purchased from Bioneer (Daejeon, South Korea). All recombinant proteins were purified using a Ni-nitrilotriacetic acid Superflow column purchased from Qiagen (Hilden, Germany). All other chemicals were sourced from Sigma-Aldrich (St. Louis, Mo). *E. coli* DH5α was used for the transformation of plasmids. *E. coli* BL21 (DE3, codon plus) harboring wild-type (WT), and NfBGL mutated genes for enzyme expression were cultured in Luria-Bertani (LB) medium supplied with 25 μg ml^{-1} of kanamycin at 37 °C. One millimolar isopropyl-β-D-thiogalactopyranoside (IPTG) was used for protein induction at 25 °C for 5–6 h.

2.2. Mutagenesis of NfBGL

Site-directed mutagenesis of NfBGL was performed using a QuikChange site-directed mutagenesis kit (Stratagene, La Jolla, CA). The pET28-*Nfbgl* with WT *bgl* gene was used as the template DNA. After confirmation by sequencing, the mutant plasmids were transformed to *E. coli* BL21, and the appeared colonies were further used for enzyme expression.

2.3. Purification of protein

WT and mutants in this study were purified using the same following experimental procedure. The collected cell pellets were washed in NaH_2PO_4 buffer (20 mM, pH 7.5). The suspended cells were kept for 30 min on ice supplied with lysozyme (1 mg ml^{-1}). The disruption of cell was performed by sonication for 5 min. The lysate was collected by centrifugation at 15,000*g* at 4 °C for 30 min for removal of cell debris and the obtained supernatant was used for further purification process. The supernatant was collected and applied on to a NiNTA column already equilibrated with binding buffer (300 mM NaCl, 50 mM NaH_2PO_4). The washing buffer (300 mM NaCl, 50 mM NaH_2PO_4, 150 mM imidazole) was used to wash away the unbound proteins. The elution buffer (300 mM NaCl, 50 mM NaH_2PO_4, 250 mM imidazole) was applied to the column to elute the bounded protein. The protein elution fractions were detected and quantitated as previously described [5,12].

2.4. Kinetic assay

The BGL activity was assayed using *p*NPG as the substrate. The BGLs assay mixtures (100 μl) consisted of 10 mM *p*NPG (final concentration), 4 μg enzyme, and 100 mM CH_3COONa buffer (pH 5.0). The enzymatic assay mixtures were incubated at 50 °C for 15 min [28]. The amount of *p*-nitrophenol produced was measured by monitoring the change in A_{415} ($\varepsilon_{415} = 17.0\ mM^{-1}\ cm^{-1}$) after adding 2 M Na_2CO_3 to each reaction mixture. The kinetic parameters for NfBGL along with its mutants were determined by incubation in potassium phosphate buffer pH 6.0 (100 mM) with increasing *p*NPG amount from 1 to 1500 mM at 40 °C. The values for K_m and V_{max} were obtained from Lineweaver–Burk plots using GraphPad Prism 5. One unit of *p*NPG hydrolyzed activity by BGL and its mutants represents the enzyme amount required to produce 1 μmol of *p*-nitrophenol per minute.

2.5. Homology modeling of the enzyme and its mutants

3D homology models of all the BGL variants were obtained by the Prime modules in Schrodinger suite [18]. Multi-template sequence and structure information was retrieved via a BLAST search to model the WT and its variants [19]. Three crystal structures of PcBGLA (PDB accession code 2E3Z, 4MDO, and 5JBK) were used as templates as they all have low sequence identities (49.37%, 53.78%, and 52.52%, respectively) with 97% query coverage (Fig. 1A) [14,20,21]. Comparative modeling was carried out to obtain the most plausible structural model of the query protein via the alignment with template protein sequences, while satisfying local molecular geometry and spatial restraints. The model sequences' fitness in the current 3D environment was assessed by the Prime application in Schrödinger Maestro Suite 2019 [18]. The evaluated 3D-models of WT and its mutants were used for following substrate docking and post-docking studies. The protein preparation wizard of Maestro [22] was utilized before docking to remove close contacts in the modeled structures and generate the OPLS2005 atom types. Substrate was docked into substrate binding pocket (SBP) of NfBGL and mutants models by the Glide XP (extra precision) docking program of Schrodinger [23]. Different poses were then generated by using random rigid-body rotations and simulated annealing of enzyme-substrate complexes. Before the course of docking process, the enzyme structure, the substrate molecules, and enzyme-substrate complexes were minimized for stable energy conformation by using an OPLS2005 [24] force field equipped in the Maestro program of Schrodinger [25]. The substrate poses were then refined with a full potential final minimization process. The desired substrate orientation with the lowest energy conformation with the enzyme model, was then used for the next round of the docking process. The docked substrate conformation was retrieved for following post-docking analysis, based on the Glide XP Score.

2.6. Thermodynamic analysis of substrate binding

2.6.1. MD simulation

MD simulation following an MM/PBSA approach was implemented to gain insights into the thermodynamics of substrate binding. The WT and its variant with a bound *p*NPG substrate, obtained from a docking calculation, were subjected to MD simulation by Gromacs5.1 [26]. Before the simulation, the protein system was cleaned, and hydrogen atoms were then added to the model using the *pdb2gmx* tool of Gromacs5.1. The Gromos54a7B force field was employed for both protein and substrate atoms. The charges for the substrate, *p*NPG, were generated using quantum mechanics (QM) optimization (6-31G++**) via the Jaguar program of Schrodinger [27]. These QM charges were used to parameterize the substrate and generate the topology through the ATB online server [28]. Each system was then solvated into a dodecahedron water box with a TIP3P water model [29]. Approximately 16 Na^+ ions were then used to neutralize each system, and periodic boundary conditions (PBCs) were maintained. A 5000 steps of Conjugate Gradient (CG) minimization and a 5000 steps of Steepest Descent (SD) minimization were employed to remove steric clashes within the protein and substrate atoms of each system. An equilibration of 1 ns at 0.5 fs time step at Normal, Temperature, and Volume (NVT) was performed. After the first equilibration, the second equilibration of 1 ns at 0.5 fs time step at Normal, Temperature, and Pressure (NPT) was performed. A 300 K temperature and 1 bar pressure was maintained with a Nosé–Hoover thermostat [30] and Parrinello-Rahman [31] pressure coupling, respectively. A production run of 10 ns was performed for each system (WT and its variants) separately after each system was well equilibrated. A

total of 40 ns MD simulation was performed in this study. Each MD simulation snapshot was extracted at every 100 ps interval of trajectories and analyzed further.

2.6.2. MM/PBSA calculation

The snapshots were extracted with every 100 ps interval for each system to calculate the binding free energy using Molecular Mechanics Poisson-Boltzmann Surface Area (MM/PBSA) strategy. A *g_mmpbsa* [32] tool was employed for the calculation. The binding (K_d) and Gibbs free energy were obtained from the binding affinity measurements by using $\Delta G = -RT \ln(1/K_d)$, where R represents the gas constant, and temperature T is in Kelvin. The binding entropy was then calculated by $\Delta S = (\Delta H - \Delta G)/T$, where ΔH is the binding enthalpy.

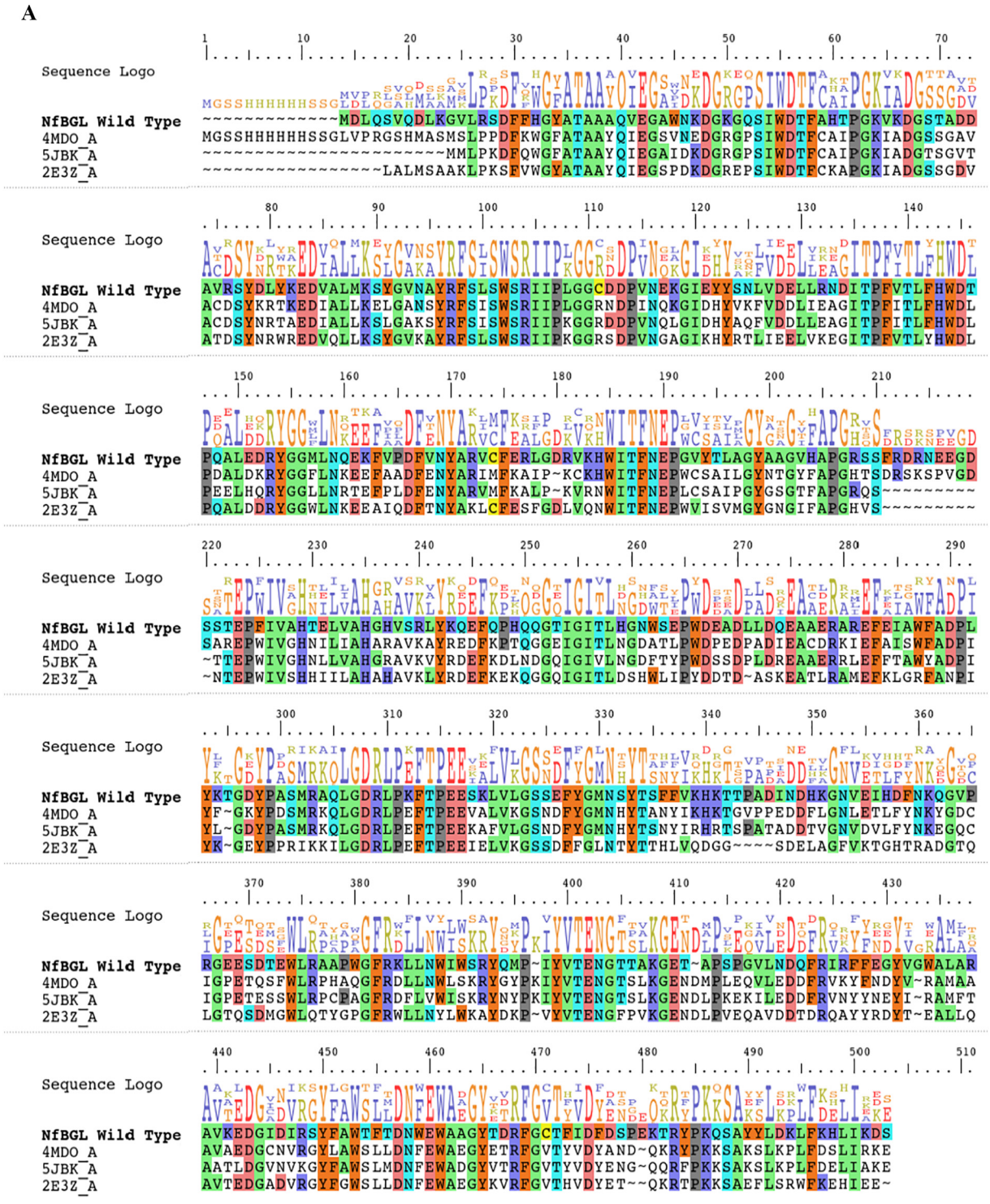

Fig. 1. (A) The multiple sequence alignment and sequence logo prediction of NfBGL with three template proteins. (B) The sequence comparison of NfBGL with other fungal BGLs by multiple sequence alignment and secondary structure prediction. The conserved residues are shown in dark green background. The Tyr320 and active sites are shown in red and yellow backgrounds, respectively. The GH 1 family consensus sequence TL/FNEP and I/VTENG is represented with a red box. Selected GH1 enzymes are from *Talaromyces emersonii, Phanerochaete chrysosporium, Coprinopsis cinerea okayama, Aspergillus niger, Ajellomyces dermatitidis, Humicola grisea,* and *Hypocrea jecorina.*

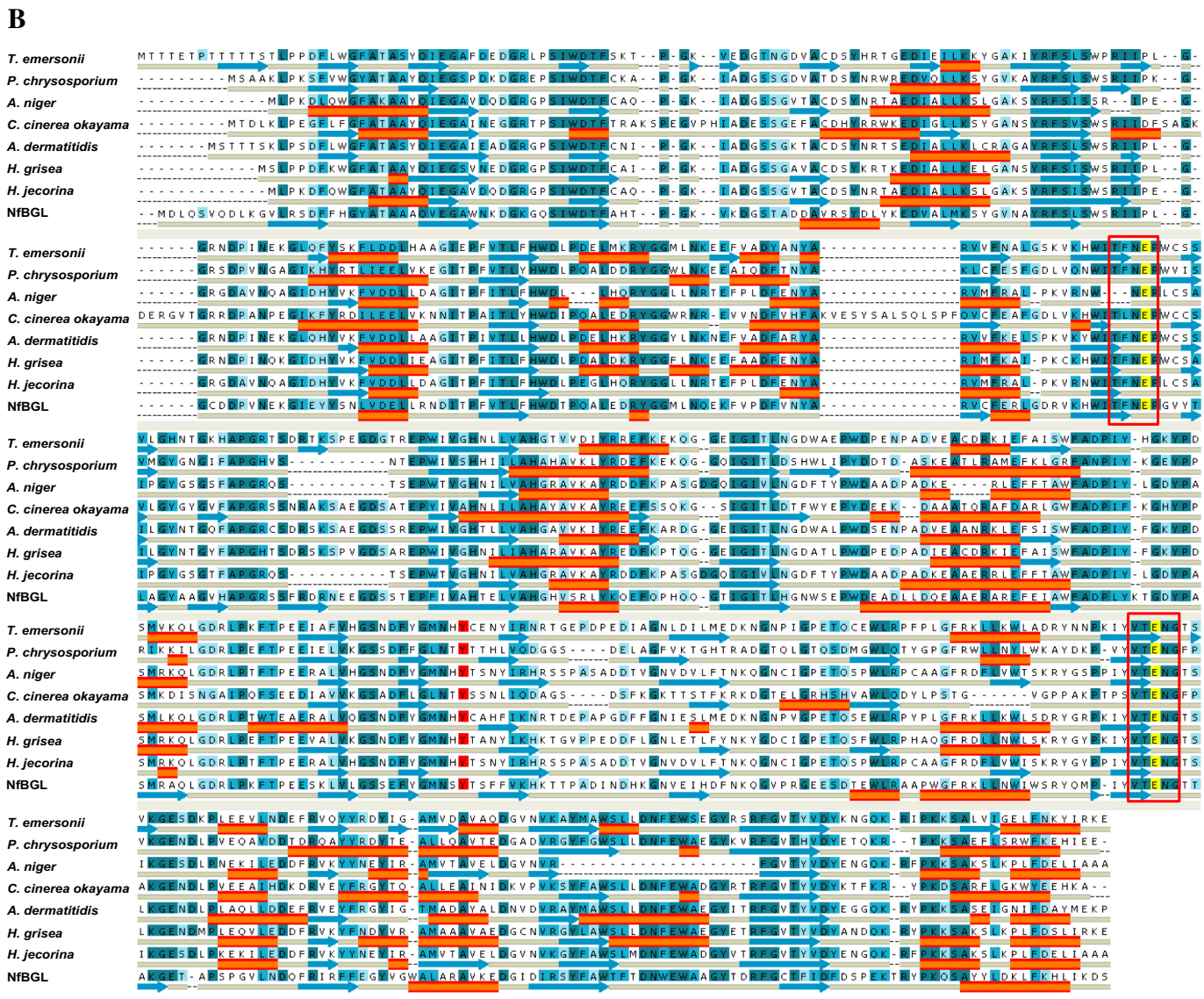

Fig. 1 (*continued*).

2.7. Analytical methods

The CD experiments were carried out at 20 °C using a Jasco J-815 spectrophotometer. Each absorbance spectrum was scanned within a range of 190 to 300 nm at a scan rate of 100 nm min^{-1}. Each averaged CD spectrum was baseline-corrected using buffer only for the control, and the measurement of each sample ellipticity was delivered in mdeg. The amino acid sequence deduced from the *bgl* gene (NfBGL) sequence of *N. fischeri* was used for comparison with related BGL by using the BLAST network service at NCBI. Next, multiple sequence alignments were carried out using the ClustalW [33].

3. Results and discussion

3.1. Sequence analysis and homology modeling

The amino acid sequence of NfBGL was aligned with other BGL sequences to find the key conserved residues in NfBGL. The sequence of deduced *bgl* gene product, NfBGL, showed identity values in the range of 43–54% with the sequences of glycoside hydrolase family 1 (GH1) enzymes from *Talaromyces emersonii* [3], *Phanerochaete chrysosporium* [34], *Aspergillus niger* [35], *Coprinopsis cinerea* okayama7#130 [36], *Ajellomyces dermatitidis* ER-3 (EEQ89827), *Humicola grisea* [37], and *Hypocrea jecorina* [37]. The cloned *Nfbgl* gene contained the two glutamate residues (Glu177 and Glu388), which are present in the conserved motifs I/VTENG and TL/FNEP [38] of GH1 enzymes (Fig. 1B).

An NfBGL homology model was constructed (Fig. S1) and then validated using a Ramachandran plot [39] by taking advantage of all three template X-ray crystal structures. The NfBGL had 95.6% residues present within the allowed area, of which 81.5% were in the favorable region. Seven residues observed were present in the Ramachandran plot outlier regions. The model evaluation was also performed via superimposition onto the selected template structure. The obtained RMSD value based on C-alpha atoms was 0.25 Å. The two glutamate residues, Glu177 and Glu388, forming an 8-fold β/α barrel structure, located in β strands 4 and 7, respectively, in the NfBGL structure appear to be involved in catalysis directly [40]. Sequence analysis and homology modeling showed that NfBGL belongs to the GH1 group.

3.2. Substrate-binding pocket (SBP)

The substrate *p*NPG was docked into the NfBGL model using the Glide XP module of the Schrodinger Suite [23]. Thirty-one residues,

which include the two active sites, Glu177 and Glu388, were found within 5 Å of the SBP (Fig. 2). Active site residues of PcBGLA [41] have previously been proposed as Glu170 and Glu365 based on the PcBGLA crystal structure information. After performing alignment with PcBGLA, the superimposition study of the NfBGL catalytic pocket with that of PcBGLA showed that the NfBGL nucleophile is Glu388 and the acid/base residue is Glu177 (Fig. S2). The *p*NPG docked NfBGL was superimposed with the *p*NPG bound PcBGLA. The superimposed structure reveals that the substrate orientation in the active site of *p*NPG-NfBGL exactly matches that of the *p*NPG-PcBGLA structure (Fig. S3). Ala screening was performed by mutating each of these two residues to Ala through the site-directed mutagenesis to further confirm this. The mutants E177A and E388A lost BGL activity, suggesting that these two residues were active site residues which are required for catalysis [40]. Sequence alignment, MD simulation, site-directed mutagenesis, and the enzyme kinetics studies showed that Glu177 and Glu388 (corresponding to Glu170 and Glu365 in PcBGLA) are active site residues in NfBGL.

The other nine conserved amino acids in the SBP were studied after investigating the role of two putative catalytic amino acids (Fig. 2). Of these nine conserved amino acids, the roles of Asn176, Asn318, and Phe454 have previously been studied in other BGLs [42]. Asn176 and Asn318 were found to be related to thermostability [13,43], and Phe454 was reported to be involved in the substrate affinity of *Pyrococcus furiosus* CelB [40]. The roles of the remaining six amino acids (His130, Tyr320, Trp361, Trp438, Glu445, and Trp446) were also studied through site-directed mutagenesis by Ala substitution. Compared with WT NfBGL, the mutation at Tyr320 significantly reduced the BGL catalytic activity (Table 1 and Fig. S4). The V_{max} value of Y320A was decreased to 2% of the WT enzyme activity when *p*NPG was used as the substrate. This significant drop in activity suggests that Tyr320 present in the SBP has an important potential role in modulating enzymatic activity. Therefore, Tyr320 was chosen for further study by site-directed mutagenesis and following investigations.

3.3. The site-directed mutagenesis of position 320

Tyrosine in position 320 was mutated to polar/charged, non-polar hydrophobic, and non-polar aromatic amino acids by site-directed mutagenesis approach. All mutants were expressed at a similar level compared to the WT NfBGL. The purified mutants (Fig. S5) exhibited similar CD spectra, within the range of 220–230 nm of the ellipticity minima of comparable amplitude (Fig. S6). This observation indicates that all the proteins were folded properly. When Tyr320 was replaced with polar and charged amino acids (Y320K and Y320E), the mutant enzymes lost activity towards *p*NPG. When Tyr320 was replaced with non-polar, aliphatic, and hydrophobic residues (Y320I, Y320V or Y320A), the activity with *p*NPG significantly decreased. The V_{max} of Y320I, Y320V, and Y320A were 71.3, 50.2, and 20.4 μmol min^{-1} mg-$protein^{-1}$, respectively, or 8.0%, 5.7%, and 2.3% of WT NfBGL activity, respectively. The functionality of the aromatic ring in Tyr320 for activity was further investigated by changing the residue to Trp or Phe. The two mutants have not drastically altered the catalytic activity, as V_{max} of Y320W and Y320F mutants was 614 and 747 μmol min^{-1} mg-$protein^{-1}$, respectively, compared with the WT. This outcome indicates that the aromatic ring present in Tyr, Trp, or Phe is important for catalytic activity of NfBGL towards *p*NPG. A similar result was obtained with another model of BGL (NfBGL595) from *N. fischeri* (XP_001258596). Tyr362, the corresponding position residue in NfBGL595, was mutated to Ala by site-directed mutagenesis and the Y362A mutant of NfBGL595 showed significantly decreased BGL activity towards *p*NPG (< 1% of the WT). The multiple sequence alignment of 250 GHs was performed and revealed that Tyr320 was completely conserved among these sequences (Fig. S7). These results indicate that Tyr320 is an important determinant of high catalytic efficiency of all GHs.

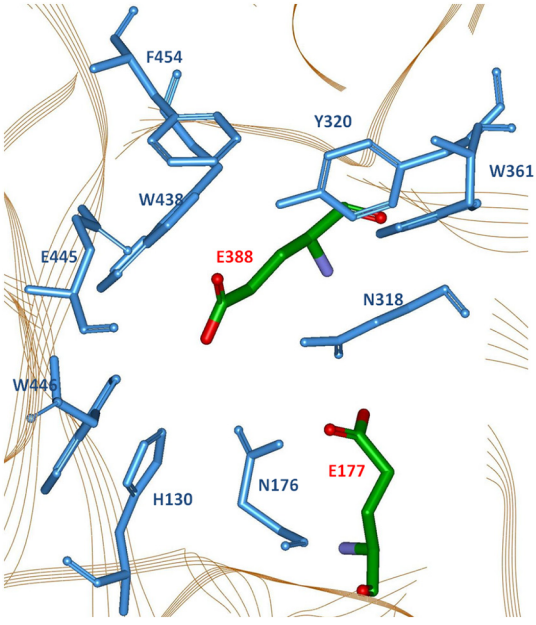

Fig. 2. The highly conserved amino acids (blue) involved in the catalytic sites (green) chosen for further site-directed mutagenesis studies.

3.4. Kinetic analysis and MD simulation studies of WT and Tyr320 mutant enzymes

The kinetic parameters of WT and mutant NfBGL enzymes were investigated by using *p*NPG as substrate. The comparison of the kinetic values of Tyr320 mutants with those of the WT NfBGL suggested the mutant enzymes with a non-polar aliphatic residue decrease k_{cat}/K_m values significantly and aromatic amino acid at position 320 is very crucial for its high catalytic efficiency and maximum turnover rate (Table 2). Molecular docking study was also performed to analyze the interaction network between the substrate and each mutated amino acid in the NfBGL mutant model (Fig. 3). MD simulation, site-directed mutagenesis and the enzyme kinetics study showed that Tyr320 interacted with the substrate *p*NPG through H-bonding and π-sigma interactions (Fig. 3A), indicating that this amino acid is important for NfBGL catalysis. These interactions between Tyr320 and the pyranose ring of *p*NPG at the SBP gate can facilitate forming the substrate proper orientation and position and stabilizing the protein-ligand complex formation. Changes in Δ(ΔG) were calculated based on the kinetic parameters of seven generated mutant enzymes (Table 2). The Y320V and Y320A mutants showed significantly lower catalytic efficiencies (18.2 and 1.4 min^{-1} mM^{-1}, respectively) with higher Δ(ΔG) values (5.71 and 7.98 kJ mol^{-1}, respectively) when compared with the WT NfBGL.

Table 1
Kinetic parameters determined for the NfBGL wild-type and mutants for *p*NPG.

Enzyme	V_{max} (μmol min^{-1} mg-$protein^{-1}$)	K_m (mM)	k_{cat} (min^{-1})
WT	886 ± 64	54.0 ± 5.9	49,600 ± 3580
E177A	ND	ND	ND
E388A	ND	ND	ND
H130A	213 ± 15	157 ± 16	11,900 ± 860
N176A	328 ± 19	116 ± 12	18,400 ± 1060
Y320A	20.4 ± 2.5	819 ± 61	1120 ± 140
W361A	659 ± 34	135 ± 11	36,900 ± 1880
W438A	399 ± 25	250 ± 21	22,300 ± 1420
E445A	625 ± 38	1450 ± 99	35,000 ± 2140
W446A	756 ± 47	121 ± 10	42,300 ± 2600
F454A	310 ± 25	109 ± 9	17,400 ± 1390

ND, not determined due to the very low activity of the enzyme.

This could be due to the disruption of π-sigma interaction and H-bonding resulting from the increased distance between the substrate and the residue of the mutants (Fig. 3C and D). However, the Y320F and Y320W mutant enzymes retained π-sigma interaction with the substrate (although the H-bonding between the *p*NPG and the residue at 320 was disappeared) and therefore showed no dramatic change in catalytic efficiency (Fig. 3B).

As shown in previous studies, GH1 enzymes adopt a double displacement mechanism (Scheme 1) by which a covalent intermediate is formed and then hydrolyzed through a transition state with significant oxocarbenium-ion-like characteristics [43]. It is known that the hydroxyl substituent at C2 plays an important role in stabilizing transition-state [44]. When *p*NPG was docked into WT NfBGL SBP, the hydroxyl groups of the C2 of substrate formed three H-bonds (3.3 Å, 3.4 Å, and 3.3 Å) with oxygen atoms present in Glu177 and Glu388 COO^- groups (Fig. 3A). The hydroxyl group of C2 made additional H-bonds (2.3 Å) with Tyr320, probably stabilizing the oxocarbenium-ion-like transition state (Scheme 1). There was no H-bonding in the Y320A mutant due to the long distance between the C2 of the active site residues Glu177 and Glu388 and the substrate (Fig. 3D). The absence of an H-bond in the Y320A mutant could explain the reduced catalytic activity for *p*NPG. When Tyr was mutated into Phe or Trp, k_{cat} remained the same since the π-sigma interaction between the substrate and the aromatic ring at the 320 position could be retained. This outcome maintained H-bonding between the C2 of the substrate and the active sites Glu177 and Glu388 with lengths of 3.5 Å, 3.8 Å, and 3.7 Å, respectively (Fig. 3B). When Tyr320 was mutated into charged amino acids, such as Lys and Glu, the mutant enzymes exhibited no BGL activity. This outcome was due to the charged amino acids disrupting the H-bonding and π-sigma interaction with the substrate. This disruption leads to the loss of H-bonding interaction between active site amino acids Glu177 and Glu388 and the C2 in the substrate.

We have also tested other substrates (cellobiose, cellotriose, and isoflavones such as daidzin and glycitin), which have more potential for industrial applications than *p*NPG. Cellobiose and cellotriose are natural substrates of BGL that are used for reducing sugar production from cellulose. Isoflavones are anti-nutritional factors that reduce the nutrient utilization [45] and exist as glycoside; meanwhile, their free forms play a role in preventing certain cancers, osteoporosis, and cardiovascular disease [46–48]. Therefore, BGLs, which convert isoflavone glycosides to free isoflavones, are important for isoflavone utilization in the food and feed industries. The wild-type NfBGL showed almost no activity for cellobiose and cellotriose; however, it displayed high bioconversion ability of isoflavone glycosides (daidzin and glycitin) into their free forms (Table 2). Therefore, catalytic efficiencies of all the NfBGL mutants for *p*NPG, daidzin, and glycitin were estimated. As shown in Table 2, Y320 NfBGL mutants showed a similar trend for the hydrolysis of *p*NPG, daidzin, and glycitin; this revealed that these mutants exhibit a common role in the reaction mechanism for the conversion of the above-mentioned substrates.

3.5. Thermodynamics of substrate binding by NfBGL variants

The thermodynamic parameters (K, K_d, and ΔG^b) for the binding of *p*NPG to NfBGL were investigated using MD and MM/PBSA using Gromacs and *g_mmpbsa* to investigate the role of Tyr320. The thermodynamic parameters of WT NfBGL, Y320F, Y320V, and Y320A with *p*NPG are compiled in Table 3. The aromatic substitution (Y320F) had little effect on the ΔG^b of NfBGL. The slight increase in ΔG^b for Y320F (-14.29 kJ mol^{-1}) was mostly due to the H-bonding disruption between the pyranose ring in *p*NPG and the amino acid at position 320. When compared to that in WT (-16.56 kJ mol^{-1}), Y320A and Y320V binding to *p*NPG showed an increase in ΔG^b of -8.5 kJ mol^{-1} and -10.85 kJ mol^{-1}, respectively. The large ΔG^b due to the aliphatic replacement of Tyr320 indicated that unfavorable contributions were significant compared with the aromatic substitution. The K_d (1.26 mM) for the WT NfBGL was much lower (12.60 and 31.42 mM) than those of the aliphatic Tyr320 variants. The increased K_d values of NfBGL variants reveal the important role of Tyr320 in the substrate binding. The binding affinity of *p*NPG to WT NfBGL was 10- and 25-fold higher than those of Y320V and Y320A, respectively. The results highlight the importance of an aromatic residue (Tyr) at position 320 in enzyme-substrate complex stabilization by π-sigma interaction and H-bonding.

The calculated ΔG^b values and catalytic efficiency obtained by experiments showed a notable correlation. It provides a feasibility for utilizing the computational calculation of ΔG^b for engineering BGL or other enzymes; this is aimed at obtaining target mutants with controlled catalytic efficiency. Therefore, in our upcoming studies, we plan to perform computational screening based on the quantitative parameter ΔG^b, which will be followed by an experimental validation; this will facilitate the screening of mutants with a higher catalytic efficiency.

4. Conclusion

The recombinant NfBGL protein from *N. fischeri* has shown high BGL activity towards *p*NPG in a previous report. In this study, we conducted a systematic analysis to investigate the molecular determinants for its high catalytic efficiency. After screening conserved residues using multiple sequence alignments, we performed MD simulation and identified the conserved residues that contacted the substrate. We also conducted individual site-directed mutagenesis as well as kinetic and thermodynamic analyses. The results indicated that position 320 in NfBGL demands an aromatic residue, which is probably required to position the pyranosyl ring of *p*NPG to form the important H-bonding and π-sigma interactions of the substrate with the active site amino acids. 3D

Table 2
Kinetic parameters of the NfBGL wild-type and Tyr320 mutants[a].

Enzyme	pNPG				Daidzin				Glycitin			
	k_{cat} (min^{-1})	K_m (mM)	k_{cat}/K_m (min^{-1} mM^{-1})	$\Delta(\Delta G)^b$ (kJ mol^{-1})	k_{cat} (min^{-1})	K_m (mM)	k_{cat}/K_m (min^{-1} mM^{-1})	$\Delta(\Delta G)^b$ (kJ mol^{-1})	k_{cat} (min^{-1})	K_m (mM)	k_{cat}/K_m (min^{-1} mM^{-1})	$\Delta(\Delta G)^b$ (kJ mol^{-1})
Wild-type	49,600	54.0	919	0	30.6	0.621	49.3	0	20.5	0.485	42.2	0
Y320F	41,900	77.1	543	1.38	24.3	0.803	30.2	1.19	12.0	0.518	23.1	1.47
Y320W	34,400	88.2	390	2.24	19.5	0.914	21.3	2.05	9.45	0.566	16.7	2.26
Y320I	3980	130	30.6	8.87	1.98	1.32	1.50	8.52	0.817	0.723	1.13	8.82
Y320V	2840	156	18.2	10.2	1.67	1.55	1.08	9.31	0.596	0.784	0.760	15.4
Y320A	1150	819	1.40	16.9	ND	ND	ND	ND	ND	ND	ND	ND
Y320E	ND[c]	ND	ND	ND	ND	ND	ND	ND	ND	ND	ND	ND
Y320K	ND	ND	ND	ND	ND	ND	ND	ND	ND	ND	ND	ND

$\Delta H = \Delta G^b - T\Delta S$, where ΔH, ΔG^b, T, and ΔS correspond to change in enthalpy, free energy of binding, temperature in Kelvin, and change in entropy, respectively.
[a] The presented k_{cat} and K_m values are the results of triplicate measurements and vary from the mean by no >15%.
[b] $\Delta(\Delta G) = -RT \cdot \ln[(k_{cat}/K_m)\text{mut}/(k_{cat}/K_m)\text{wt}]$, where R is the ideal gas constant, and T is the temperature in Kelvin.
[c] ND, not determined because of its low activity.

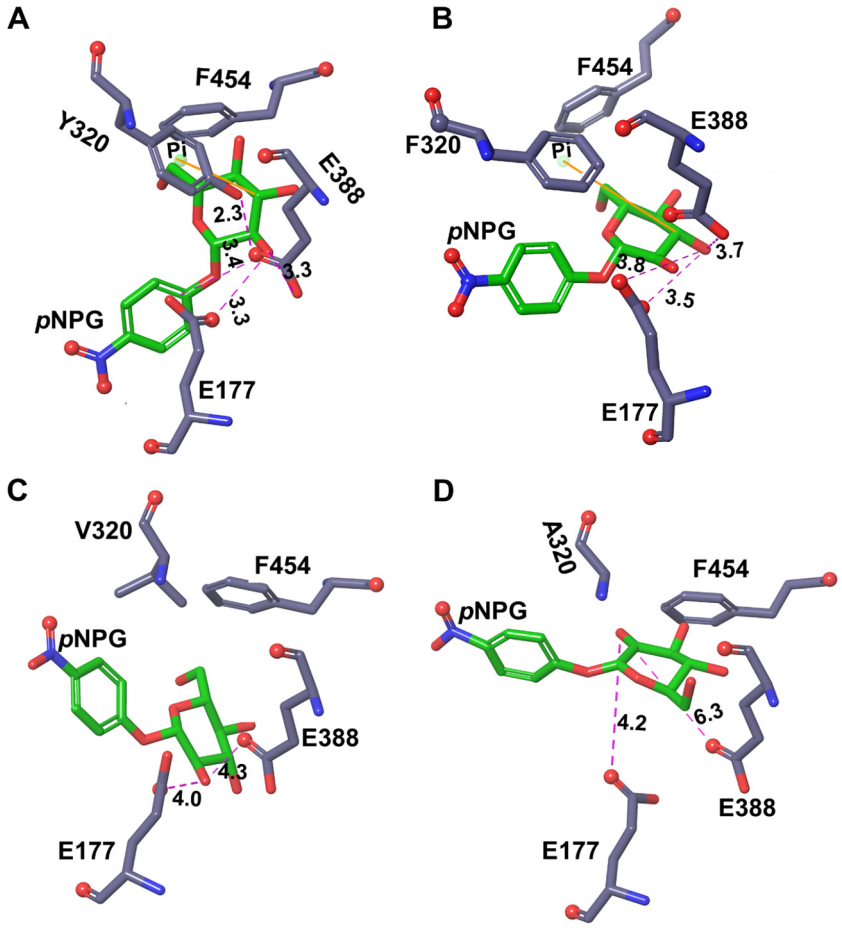

Fig. 3. The active sites with bound substrate *p*NPG present in the NfBGL and the mutants. *p*NPG was used to dock into substrate binding pocket of (A) NfBGL, (B) Y320F, (C) Y320V, and (D) Y320A.

structural models of mutants revealed a change in the location of *p*NPG in the active site. This change modified the distance between the active site residues and the substrate, resulting in the less efficient hydrolysis of *p*NPG by the NfBGL mutants, compared to that by WT NfBGL. These changes may induce disruption of the H-bonding or π-sigma interaction between the amino acid at position 320 and the substrate, resulting in

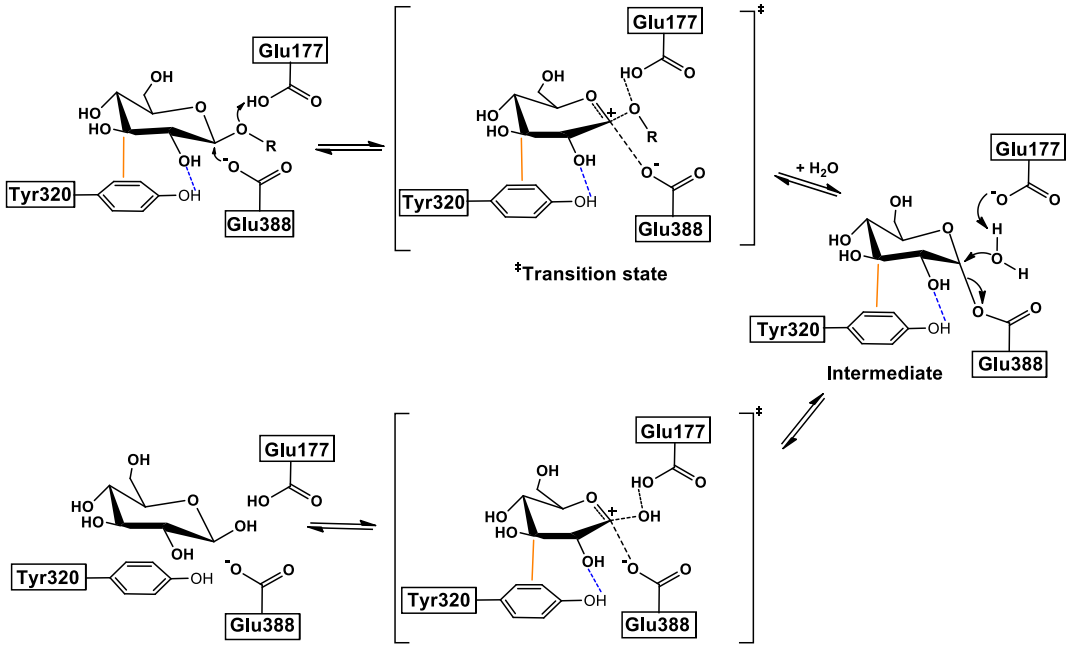

Scheme 1. A suggested mechanism for NfBGL along with the role of Tyr320 in the stabilization of the enzyme-substrate complex. Dotted line: H-bonding, solid line: π-sigma interaction.

Table 3
The thermodynamic parameters determined by MD simulation and MM/PBSA.

Enzyme	−TΔS	ΔH	K_d (mM)	ΔG^b	$\Delta(\Delta G^b)$
Wild-type	48.68	32.12	1.26 ± 0.23	−16.57	0.000
Y320F	23.31	9.02	3.15 ± 0.34	−14.29	2.273
Y320V	14.88	4.02	12.60 ± 1.31	−10.85	5.713
Y320A	24.32	15.74	31.42 ± 2.30	−8.585	7.980

Energy parameters are in kJ mol^{-1}.
$\Delta G^b = -RT \cdot \ln K$.
$\Delta(\Delta G^b) = \Delta G^b$ (mutant) − ΔG^b (WT).

an unstable oxocarbenium-ion-like transition state and an unfavorable nucleophilic attack orientation via the carboxyl group of Glu388. The amino acid Tyr320 is a completely conserved residue in all GHs, indicating that Tyr in this position could be an important determinant of the catalytic efficiency of all GHs.

CRediT authorship contribution statement

Ramasamy Shanmugam: Conceptualization, Methodology, Writing - original draft.**In-Won Kim:** Conceptualization, Methodology, Writing - original draft.**Manish K. Tiwari:** Conceptualization, Methodology, Writing - original draft.**Hui Gao:** Visualization, Investigation.**Primata Mardina:** Visualization, Investigation.**Devashish Das:** Software, Validation, Writing - review & editing.**Anurag Kumar:** Software, Validation, Writing - review & editing.**Marimuthu Jeya:** Visualization, Investigation, Software, Validation, Writing - review & editing.**Sang-Yong Kim:** Visualization, Investigation, Software, Validation, Writing - review & editing.**Young Sin Kim:** Software, Validation, Writing - review & editing.**Jung-Kul Lee:** Supervision, Writing - review & editing.

Acknowledgments

This paper was supported by Konkuk University in 2017.

Appendix A. Supplementary data

Supplementary data to this article can be found online at https://doi.org/10.1016/j.ijbiomac.2020.02.117.

References

[1] J.R.K. Cairns, A. Esen, β-Glucosidases, Cell. Mol. Life Sci. 67 (2010) 3389–3405, https://doi.org/10.1007/s00018-010-0399-2.
[2] D. Mamma, D.G. Hatzinikolaou, P. Christakopoulos, Biochemical and catalytic properties of two intracellular β-glucosidases from the fungus Penicillium decumbens active on flavonoid glucosides, J. Mol. Catal. B Enzym. 27 (2004) 183–190, https://doi.org/10.1016/j.molcatb.2003.11.011.
[3] P. Murray, N. Aro, C. Collins, A. Grassick, M. Penttilä, M. Saloheimo, M. Tuohy, Expression in Trichoderma reesei and characterisation of a thermostable family 3 β-glucosidase from the moderately thermophilic fungus Talaromyces emersonii, Protein Expr. Purif. 38 (2004) 248–257, https://doi.org/10.1016/j.pep.2004.08.006.
[4] G. Singh, A.K. Verma, V. Kumar, Catalytic properties, functional attributes and industrial applications of β-glucosidases, 3 Biotech 6 (2016) 3, https://doi.org/10.1007/s13205-015-0328-z.
[5] P. Ramachandran, M.K. Tiwari, R.K. Singh, J.R. Haw, M. Jeya, J.K. Lee, Cloning and characterization of a putative β-glucosidase (NfBGL595) from *Neosartorya fischeri*, Process Biochem. 47 (2012) 99–105, https://doi.org/10.1016/j.procbio.2011.10.015.
[6] M. Jeya, A.R. Joo, K.M. Lee, M.K. Tiwari, K.M. Lee, S.H. Kim, J.K. Lee, Characterization of β-glucosidase from a strain of Penicillium purpurogenum KJS506, Appl. Microbiol. Biotechnol. 86 (2010) 1473–1484, https://doi.org/10.1007/s00253-009-2395-8.
[7] T. Fukuda, M. Kato-Murai, T. Kadonosono, H. Sahara, Y. Hata, S.I. Suye, M. Ueda, Enhancement of substrate recognition ability by combinatorial mutation of β-glucosidase displayed on the yeast cell surface, Appl. Microbiol. Biotechnol. 76 (2007) 1027–1033, https://doi.org/10.1007/s00253-007-1070-1.
[8] J. Hong, H. Tamaki, H. Kumagai, Cloning and functional expression of thermostable β-glucosidase gene from Thermoascus aurantiacus, Appl. Microbiol. Biotechnol. 73 (2007) 1331–1339, https://doi.org/10.1007/s00253-006-0618-9.
[9] W. Liu, J. Hong, D.R. Bevan, Y.H.P. Zhang, Fast identification of thermostable beta-glucosidase mutants on cellobiose by a novel combinatorial selection/screening approach, Biotechnol. Bioeng. 103 (2009) 1087–1094, https://doi.org/10.1002/bit.22340.
[10] K.B.R.M. Krogh, P.V. Harris, C.L. Olsen, K.S. Johansen, J. Hojer-Pedersen, J. Borjesson, L. Olsson, Characterization and kinetic analysis of a thermostable GH3 β-glucosidase from Penicillium brasilianum, Appl. Microbiol. Biotechnol. 86 (2010) 143–154, https://doi.org/10.1007/s00253-009-2181-7.
[11] N.P.T. Nguyen, K.M. Lee, K.M. Lee, I.W. Kim, Y.S. Kim, M. Jeya, J.K. Lee, One-step purification and characterization of a β-1,4-glucosidase from a newly isolated strain of *Stereum hirsutum*, Appl. Microbiol. Biotechnol. 87 (2010) 2107–2116, https://doi.org/10.1007/s00253-010-2668-2.
[12] M.K. Tiwari, K.M. Lee, D. Kalyani, R.K. Singh, H. Kim, J.K. Lee, P. Ramachandran, Role of Glu445 in the substrate binding of β-glucosidase, Process Biochem. 47 (2012) 2365–2372, https://doi.org/10.1016/j.procbio.2012.09.015.
[13] T. Jeoh, J.O. Baker, M.K. Ali, M.E. Himmel, W.S. Adney, β-D-Glucosidase reaction kinetics from isothermal titration microcalorimetry, Anal. Biochem. 347 (2005) 244–253, https://doi.org/10.1016/j.ab.2005.09.031.
[14] Y. Nijikken, T. Tsukada, K. Igarashi, M. Samejima, T. Wakagi, H. Shoun, S. Fushinobu, Crystal structure of intracellular family 1 β-glucosidase BGL1A from the basidiomycete Phanerochaete chrysosporium, FEBS Lett. 581 (2007) 1514–1520, https://doi.org/10.1016/j.febslet.2007.03.009.
[15] J. Zouhar, J. Vévodová, J. Marek, J. Damborský, X.-D. Su, B. Brzobohatý, Insights into the functional architecture of the catalytic center of a maize β-glucosidase Zm-p60.1, Plant Physiol. 127 (3) (2001) 973, https://doi.org/10.1104/pp.010712.
[16] W.P. Burmeister, S. Cottaz, H. Driguez, R. Iori, S. Palmieri, B. Henrissat, The crystal structures of Sinapis alba myrosinase and a covalent glycosyl–enzyme intermediate provide insights into the substrate recognition and active-site machinery of an S-glycosidase, Structure 5 (1997) 663–676, https://doi.org/10.1016/s0969-2126(97)00221-9.
[17] M. Sue, K. Yamazaki, S. Yajima, T. Nomura, T. Matsukawa, H. Iwamura, T. Miyamoto, Molecular and structural characterization of hexameric β-D-glucosidases in wheat and rye, Plant Physiol. 141 (2006) 1237–1247, https://doi.org/10.1104/pp.106.077693.
[18] M.P. Jacobson, D.L. Pincus, C.S. Rapp, T.J.F. Day, B. Honig, D.E. Shaw, R.A. Friesner, A hierarchical approach to all-atom protein loop prediction, Proteins Struct. Funct. Bioinforma. 55 (2004) 351–367, https://doi.org/10.1002/prot.10613.
[19] S.F. Altschul, T.L. Madden, A.A. Schäffer, J. Zhang, Z. Zhang, W. Miller, D.J. Lipman, Gapped BLAST and PSI-BLAST: a new generation of protein database search programs, Nucleic Acids Res. 25 (1997) 3389–3402, https://doi.org/10.1093/nar/25.17.3389.
[20] P.O. de Giuseppe, T. de A.C.B. Souza, F.H.M. Souza, L.M. Zanphorlin, C.B. Machado, R.J. Ward, J.A. Jorge, R. dos P.M. Furriel, M.T. Murakami, Structural basis for glucose tolerance in GH1 β-glucosidases, Acta Crystallogr. Sect. D Biol. Crystallogr. 70 (2014) 1631–1639, https://doi.org/10.1107/s1399004714006920.
[21] R.N. Florindo, V.P. Souza, H.S. Mutti, C. Camilo, L.R. Manzine, S.R. Marana, I. Polikarpov, A.S. Nascimento, Structural insights into β-glucosidase transglycosylation based on biochemical, structural and computational analysis of two GH1 enzymes from *Trichoderma harzianum*, New Biotechnol. 40 (2018) 218–227, https://doi.org/10.1016/j.nbt.2017.08.012.
[22] J.C. Shelley, A. Cholleti, L.L. Frye, J.R. Greenwood, M.R. Timlin, M. Uchimaya, Epik: a software program for pKa prediction and protonation state generation for drug-like molecules, J. Comput. Aided Mol. Des. 21 (2007) 681–691, https://doi.org/10.1007/s10822-007-9133-z.
[23] R.A. Friesner, J.L. Banks, R.B. Murphy, T.A. Halgren, J.J. Klicic, D.T. Mainz, M.P. Repasky, E.H. Knoll, M. Shelley, J.K. Perry, D.E. Shaw, P. Francis, P.S. Shenkin, Glide: a new approach for rapid, accurate docking and scoring. 1. Method and assessment of docking accuracy, J. Med. Chem. 47 (2004) 1739–1749, https://doi.org/10.1021/jm0306430.
[24] J.L. Banks, H.S. Beard, Y. Cao, A.E. Cho, W. Damm, R. Farid, A.K. Felts, T.A. Halgren, D.T. Mainz, J.R. Maple, R. Murphy, D.M. Philipp, M.P. Repasky, L.Y. Zhang, B.J. Berne, R.A. Friesner, E. Gallicchio, R.M. Levy, Integrated modeling program, applied chemical theory (IMPACT), J. Comput. Chem. 26 (2005) 1752–1780, https://doi.org/10.1002/jcc.20292.
[25] L. Schrödinger, Schrödinger Release 2019–1: Maestro, 2019.
[26] M.J. Abraham, T. Murtola, R. Schulz, S. Páll, J.C. Smith, B. Hess, E. Lindahl, GROMACS: high performance molecular simulations through multi-level parallelism from laptops to supercomputers, SoftwareX. 1–2 (2015) 19–25, https://doi.org/10.1016/j.softx.2015.06.001.
[27] A.D. Bochevarov, E. Harder, T.F. Hughes, J.R. Greenwood, D.A. Braden, D.M. Philipp, D. Rinaldo, M.D. Halls, J. Zhang, R.A. Friesner, Jaguar: a high-performance quantum chemistry software program with strengths in life and materials sciences, Int. J. Quantum Chem. 113 (2013) 2110–2142, https://doi.org/10.1002/qua.24481.
[28] A.K. Malde, L. Zuo, M. Breeze, M. Stroet, D. Poger, P.C. Nair, C. Oostenbrink, A.E. Mark, An automated force field topology builder (ATB) and repository: version 1.0, J. Chem. Theory Comput. 7 (2011) 4026–4037, https://doi.org/10.1021/ct200196m.
[29] P. Mark, L. Nilsson, Structure and dynamics of the TIP3P, SPC, and SPC/E water models at 298 K, J. Phys. Chem. A 105 (2001) 9954–9960, https://doi.org/10.1021/jp003020w.
[30] W.G. Hoover, Constant-pressure equations of motion, Phys. Rev. A 34 (1986) 2499–2500, https://doi.org/10.1103/PhysRevA.34.2499.
[31] M. Parrinello, A. Rahman, Crystal structure and pair potentials: a molecular-dynamics study, Phys. Rev. Lett. 45 (1980) 1196–1199, https://doi.org/10.1103/PhysRevLett.45.1196.
[32] R. Kumari, R. Kumar, A. Lynn, A. Lynn, *g_mmpbsa*—a GROMACS tool for high-throughput MM-PBSA calculations, J. Chem. Inf. Model. 54 (2014) 1951–1962, https://doi.org/10.1021/ci500020m.
[33] J.D. Thompson, T.J. Gibson, D.G. Higgins, Multiple sequence alignment using ClustalW and ClustalX, Curr. Protoc. Bioinforma. 0 (2003) 2.3.1–2.3.22, https://doi.org/10.1002/0471250953.bi0203s00.

[34] T. Tsukada, K. Igarashi, M. Yoshida, M. Samejima, Molecular cloning and characterization of two intracellular β-glucosidases belonging to glycoside hydrolase family 1 from the basidiomycete Phanerochaete chrysosporium, Appl. Microbiol. Biotechnol. 73 (2006) 807–814, https://doi.org/10.1007/s00253-006-0526-z.

[35] H.F. Seidle, K. McKenzie, I. Marten, O. Shoseyov, R.E. Huber, Trp-262 is a key residue for the hydrolytic and transglucosidic reactivity of the Aspergillus niger family 3 β-glucosidase: substitution results in enzymes with mainly transglucosidic activity, Arch. Biochem. Biophys. 444 (2005) 66–75, https://doi.org/10.1016/j.abb.2005.09.013.

[36] J.E. Stajich, S.K. Wilke, D. Ahren, C.H. Au, B.W. Birren, M. Borodovsky, C. Burns, B. Canback, L.A. Casselton, C.K. Cheng, J. Deng, F.S. Dietrich, D.C. Fargo, M.L. Farman, A.C. Gathman, J. Goldberg, R. Guigo, P.J. Hoegger, J.B. Hooker, A. Huggins, T.Y. James, T. Kamada, S. Kilaru, C. Kodira, U. Kues, D. Kupfer, H.S. Kwan, A. Lomsadze, W. Li, W.W. Lilly, L.-J. Ma, A.J. Mackey, G. Manning, F. Martin, H. Muraguchi, D.O. Natvig, H. Palmerini, M.A. Ramesh, C.J. Rehmeyer, B.A. Roe, N. Shenoy, M. Stanke, V. Ter-Hovhannisyan, A. Tunlid, R. Velagapudi, T.J. Vision, Q. Zeng, M.E. Zolan, P.J. Pukkila, Insights into evolution of multicellular fungi from the assembled chromosomes of the mushroom Coprinopsis cinerea (Coprinus cinereus), Proc. Natl. Acad. Sci. 107 (2010) 11889–11894, https://doi.org/10.1073/pnas.1003391107.

[37] S. Takashima, A. Nakamura, M. Hidaka, H. Masaki, T. Uozumi, Molecular cloning and expression of the novel fungal β-glucosidase genes from Humicola grisea and Trichoderma reesei, J. Biochem. 125 (4) (1999) 728–736, https://doi.org/10.1093/oxfordjournals.jbchem.a022343.

[38] P. Toonkool, P. Metheenukul, P. Sujiwattanarat, P. Paiboon, N. Tongtubtim, M. Ketudat-Cairns, J. Ketudat-Cairns, J. Svasti, Expression and purification of dalcochinase, a β-glucosidase from Dalbergia cochinchinensis Pierre, in yeast and bacterial hosts, Protein Expr. Purif. 48 (2006) 195–204, https://doi.org/10.1016/j.pep.2006.05.011.

[39] G.N. Ramachandran, C. Ramakrishnan, V. Sasisekharan, Stereochemistry of polypeptide chain configurations, J. Mol. Biol. 7 (1963) 95–99, https://doi.org/10.1016/S0022-2836(63)80023-6.

[40] T. Kaper, J.H.G. Lebbink, J. Pouwels, J. Kopp, G.E. Schulz, J. van der Oost, W.M. de Vos, Comparative structural analysis and substrate specificity engineering of the hyperthermostable β-glucosidase CelB from Pyrococcus furiosus †, Biochemistry 39 (2000) 4963–4970, https://doi.org/10.1021/bi992463r.

[41] B.-J. Kim, S.P. Singh, K. Hayashi, Characteristics of chimeric enzymes constructed between Thermotoga maritima and Agrobacterium tumefaciens β-glucosidases: role of C-terminal domain in catalytic activity, Enzym. Microb. Technol. 38 (2006) 952–959, https://doi.org/10.1016/j.enzmictec.2005.08.038.

[42] S.C. Lovell, I.W. Davis, W.B. Arendall, P.I.W. de Bakker, J.M. Word, M.G. Prisant, J.S. Richardson, D.C. Richardson, Structure validation by Cα geometry: ϕ,ψ and Cβ deviation, Proteins Struct. Funct. Bioinforma. 50 (2003) 437–450, https://doi.org/10.1002/prot.10286.

[43] G. Davies, B. Henrissat, Structures and mechanisms of glycosyl hydrolases, Structure 3 (1995) 853–859, https://doi.org/10.1016/S0969-2126(01)00220-9.

[44] T. Barrett, C.G. Suresh, S.P. Tolley, E.J. Dodson, M.A. Hughes, The crystal structure of a cyanogenic β-glucosidase from white clover, a family 1 glycosyl hydrolase, Structure 3 (1995) 951–960, https://doi.org/10.1016/S0969-2126(01)00229-5.

[45] K.O. Soetan, O.E. Oyewole, The need for adequate processing to reduce the antinutritional factors in plants used as human foods and animal feeds: a review, Afr. J. Food Sci. 3 (9) (2009) 223–232.

[46] D. Goodman-Gruen, D. Kritz-Silverstein, Usual dietary isoflavone intake is associated with cardiovascular disease risk factors in postmenopausal women, J. Nutr. 131 (4) (2001) 1202–1206, https://doi.org/10.1093/jn/131.4.1202.

[47] M.H. Ravindranath, S. Muthugounder, N. Presser, S. Viswanathan, Anticancer therapeutic potential of soy isoflavone, genistein, in: E.L. Cooper, N. Yamaguchi (Eds.), Complementary and Alternative Approaches to Biomedicine, Springer US, Boston, MA 2004, pp. 121–165, https://doi.org/10.1007/978-1-4757-4820-8_11.

[48] L.C. Kuo, W.Y. Cheng, R.-Y. Wu, C.J. Huang, K.T. Lee, Hydrolysis of black soybean isoflavone glycosides by *Bacillus subtilis* natto, Appl. Microbiol. Biotechnol. 73 (2) (2006) 314–320, https://doi.org/10.1007/s00253-006-0474-7.